3-D Finite-Element Models of Human and Monkey Fingertips to Investigate the Mechanics of Tactile Sense

Kiran Dandekar

Balasundar I. Raju

Mandayam A. Srinivasan*

The Touch Lab
Department of Mechanical Engineering, and
The Research Laboratory of Electronics
Massachusetts Institute of Technology
Cambridge, MA 02139

The biomechanics of skin and underlying tissues plays a fundamental role in the human sense of touch. It governs the mechanics of contact between the skin and an object, the transmission of the mechanical signals through the skin, and their transduction into neural signals by the mechanoreceptors. To better understand the mechanics of touch, it is necessary to establish quantitative relationships between the loads imposed on the skin by an object, the state of stresses/strains at mechanoreceptor locations, and the resulting neural response. Towards this goal, 3-D finite-element models of human and monkey fingertips with realistic external geometries were developed. By computing fingertip model deformations under line loads, it was shown that a multi-layered model was necessary to match previously obtained in vivo data on skin surface displacements. An optimal ratio of elastic moduli of the layers was determined through numerical experiments whose results were matched with empirical data. Numerical values of the elastic moduli of the skin layers were obtained by matching computed results with empirically determined force-displacement relationships for a variety of indentors. Finally, as an example of the relevance of the model to the study of tactile neural response, the multilayered 3-D finite-element model was shown to be able to predict the responses of the slowly adapting type I (SA-I) mechanoreceptors to indentations by complex object shapes.
[DOI: 10.1115/1.1613673]

1 Introduction

Just as the optics of the eye and acoustics of the ear are fundamental to understand our senses of vision and hearing, the mechanics of the skin is important to understand our sense of touch. When an object is explored and manipulated with the hand, the peripheral neural signals received and used by the brain to infer the properties of the object in contact with the fingertips are the trains of neural impulses generated by the population of mechanoreceptors embedded in the skin. These spatially distributed mechanoreceptors transduce the mechanical state (stresses, strains, or a combination) in their respective neighborhoods and generate the neural impulses. However, the mechanical state at receptor locations is not empirically observable with the current technology. Therefore, there is a need for the development of reliable models of the fingertip to investigate the mechanistic bases of touch.

The structure as well as the material behavior of the primate fingertip is complex, owing to irregularly shaped layers of tissues that exhibit nonlinear force-displacement relations, anisotropy, rate and time dependence. Lanir [1] has compiled various forms of constitutive models for skin (approximately 25 in number) and it is unlikely that a common agreement will emerge in the near future. Also most of the available material data are from tension tests on excised specimens, the properties of which are known to be different from that of in vivo tissues due to the loss of natural tension, absence of blood flow, and specimen preparation effects. Moreover, no reliable data exists on the geometry and material properties of individual layers of tissues that make up the fingerpad. Therefore, our approach is a combination of mechanics and systems modeling, which treats the fingertip as a black box to develop reduced order mechanistic models whose input-output relationship matches the corresponding biomechanical data [2]. The number of model parameters whose values are altered to achieve the match are kept to a minimum. This is consistent with our view that a model need not and should not incorporate complexities unless it is forced to do so.

We first developed the ''waterbed'' model, which idealized the fingertip as an elastic membrane representing the skin enclosing an incompressible fluid representing the subcutaneous tissues [3]. Although the model accurately predicted in vivo measurements of skin surface deflection profiles under line loads, it failed to predict the observed spatial distribution of mechanoreceptor responses. In contrast, a sequence of 2-D plane strain models composed of a homogeneous linear elastic material failed to predict the deflection profiles under line loads, but matched the spatial response profiles of SA-I mechanoreceptors under rectangular gratings very well [2,4,5]. From these studies, we concluded that model geometry is important in predicting mechanoreceptor responses. Further, to match both the surface deflection and mechanoreceptor response profiles, we hypothesized that a thick elastic layer with embedded receptors and supported by an incompressible fluid or a soft solid is needed [2].

Subsequently, several researchers have attempted to model the mechanical aspects of the fingerpad. Serina et al. [6] modeled the finger as an inflated ellipsoidal membrane for the epidermis filled with an incompressible fluid modeling the subcutaneous fat, which is similar to our earlier waterbed model [3]. Although this model accounted for empirical data described in [7], its formulation limits it to loading by flat-plate indentors. Maeno et al. [8,9] developed a two-dimensional inhomogeneous finite element model of the fingerpad, but no empirical verifications of the capabilities of the model were done, and the elastic constants were determined using a single cadaver tissue. Pawluk and Howe [10] used a lumped parameter model for predicting the dynamic force-displacement response of the finger, but the model is incapable of determining the spatial distribution of surface pressure, or the distribution of the mechanical stresses and strains in the vicinity of the mechanoreceptors.

*Corresponding address: Massachusetts Institute of Technology, Room 36-791, 50 Vassar Street, Cambridge MA 02139; Phone: 617-253-2512; Fax: 617-258-7003; e-mail: srini@mit.edu.

Contributed by the Bioengineering Division for publication in the JOURNAL OF BIOMECHANICAL ENGINEERING. Manuscript received by the Bioengineering Division July 11, 2002; revision received April 28, 2003. Associate Editor: C. R. Jacobs.

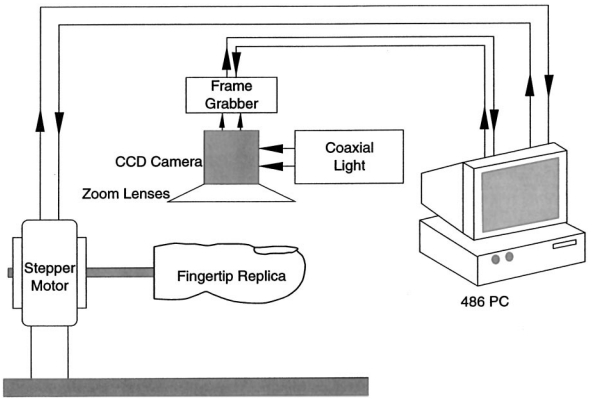

Fig. 1 Experimental setup used for extracting borders from the epoxy replicas of monkey and human fingertips

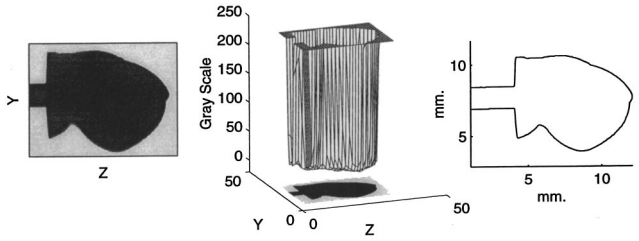

Fig. 2 Extraction of the fingertip boundary from images of the fingertip replicas. The raw image shown in the left panel is the image as acquired by the frame grabber. The 2-D histogram is shown in the middle panel and shows a clear distinction between the gray-scale values of the fingertip and the background. The extracted border is shown in the right panel.

In this paper, we develop models that take into account the full 3-D geometry of the human and macaque monkey fingertips, including their inhomogeneous layered structure. In Section 2, we describe the use of a custom-built video microscopy system to obtain accurate external geometry of human and monkey fingertips. The development of finite-element models based on this data is described in Section 3. Section 4 describes the determination of the material properties of the fingerpad tissues to be used in the finite-element models. By matching empirical data on surface deflection profiles with those of the finite-element-model predictions, a three-layered model for the fingerpad with specified ratios of the elastic constants of each layer is developed. The numerical values of the elastic constants of the layers are then determined by matching the empirically observed force-displacement relationships under loading by various indentors with those of model predictions. In Section 5, as an example of the relevance of the model to gain insights into tactile neural response, this model is shown to predict the data from neurophysiological experiments on spatial receptor response profiles of SA-I mechanoreceptors under static indentation of complex shapes. The paper ends with a discussion of the results and significance of the model.

2 Determination of Human and Monkey Fingertip Geometries

A videomicroscopy setup, shown schematically in Fig. 1, was used to acquire a sequence of high contrast 2-D images of primate fingertip replicas at various orientations. The system consisted of a monochrome CCD camera with zoom lenses, coaxial and fiber-optic light sources, a frame grabber, and a PC. Custom software was developed to store the acquired images on the computer. The border of the fingertip in each image was extracted and all such borders from different orientations were combined to reconstruct the 3-D geometry of monkey and human fingertips. Replicas were used because preliminary experiments with human fingertips in vivo showed that involuntary motions of the subject introduced errors in the angular position of the fingertip. Dental molding material was used to prepare molds for the replicas, into which epoxy resin was poured, allowed to harden, and removed. To obtain replicas of monkey fingertips, tranquilized *Macaca fascicularis* monkeys were used and the same procedure was followed. These casts were found to be extremely accurate in reproducing the finger print ridges, details of the nail, and wrinkles on the skin. The fingertip replicas were painted black to increase the contrast in the images, which was necessary to extract the correct border from the image. A central hole was drilled at the proximal end of each epoxy replica and a steel rod was inserted and glued to the replica, which then served as the axis of the fingertip. Using this rod, the fingertip replicas were mounted on a stepper motor, which was also controlled by the PC. The stepper motor had a resolution of 400 counts per revolution and, thus, the replicas could be rotated about the axis in about 0.9° steps. Typically, 100 images at distinct orientations were obtained for each fingertip.

Once the images were obtained, the border of the fingertip was extracted as shown in Fig. 2. A raw image acquired in the experiment is shown in the left panel. In the central panel, the gray-scale value at each point in the image is plotted on the vertical axis. The border, extracted using thresholding, is shown in the right panel. The longitudinal sections obtained by extracting the borders from the images are shown for four sections in the left panel of Fig. 3. The borders are plotted at the respective orientations at which they were acquired. Although it is possible to construct a 3-D solid representing the fingertip from the longitudinal sections, it was more convenient to obtain cross-sections for ease in defining several layers of tissues within the fingertip. Hence, the longitudinal sections were converted to a data set consisting of axial cross-sections spaced between 0.5–2.0 mm apart. Several axial cross-sections of the monkey fingertip generated using this algorithm are shown in the right panel of Fig. 3.

3 Development of Finite-Element Models of Human and Monkey Fingertips

The 2-D sections were then imported into a solid modeler software (Patran, McNeal-Schwendler Corporation, Santa Ana, CA) and parametric surface primitives of the 3-D solid model were defined in each cross-section. Five layers were defined in each of the cross-sections to model different tissue layers in the fingertip. The dimensions of the layers were chosen from the available data on the gross thicknesses of the layers of skin. At the center of the fingerpad, the skin was modeled with two layers of 0.5 and 1.0 mm thickness, corresponding to the epidermis and dermis respectively. The dimensions of the bone in the distal phalanx were extracted from published X-ray images and the thickness of the bone as a percentage of the fingertip diameter was calculated at various locations along the finger axis. This was used in determining the size of the innermost layer of the cross-section, which corresponded to the bone. The bone in the primate distal phalanx is axially shifted towards the nail, away from the geometrical center of the cross-sections of the fingertip, and this offset was taken into account in defining the bone location in each of the cross-sections. Two more intermediate layers were generated between the skin and the bone to model the adipose tissues and the fibrous matrix. All the internal layers, except the innermost layer corresponding to the bone, were generated by scaling the profile of the cross-section. Scaling factors were defined as the ratio of the thickness of each layer and the thickness of the fingertip at three representative cross-sections, and the same factors were then used for all the cross-sections. The resulting solid model consisted of a collection of patches and hyperpatches that were the 2-D and 3-D parametric primitives used in the algebraic representation of surfaces and solids, respectively. To facilitate definition and refinement of the finite-element mesh in the solid model, each axial cross-section was represented in polar coordinates (r,θ) with the

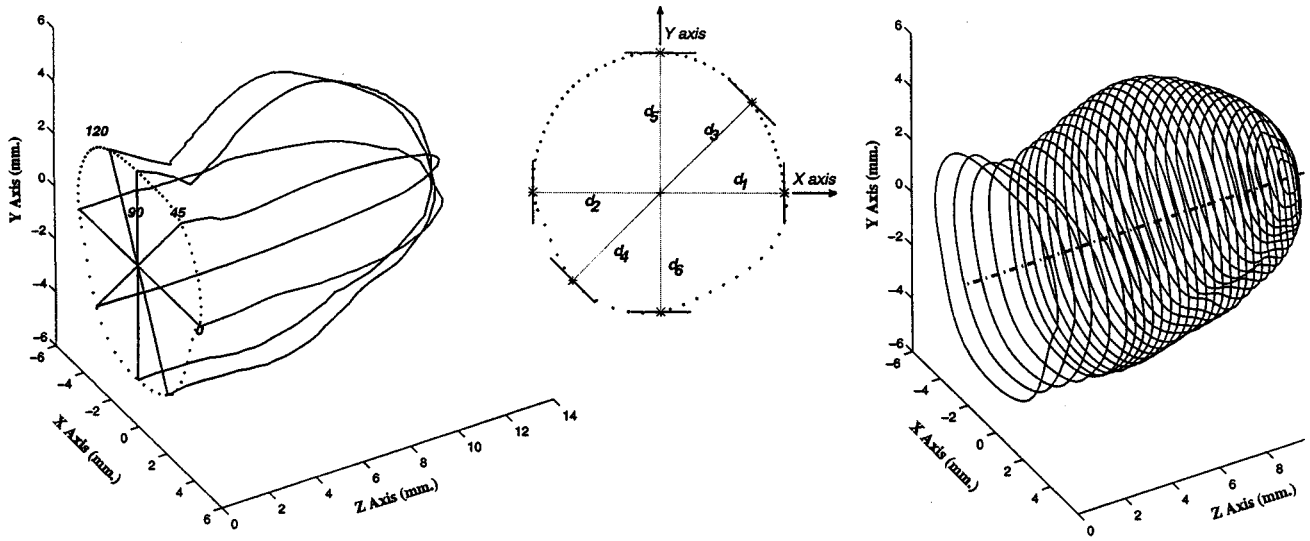

Fig. 3 The algorithm for reconstruction of the 3-D fingertip. Four extracted fingertip boundaries at 0, 45, 90, and 120 deg are shown on the left. An axial cross-section reconstructed from the extracted borders is shown in the middle. As shown on the right, the set of all such cross-sections define the external geometry of the monkey fingertip and a solid can be generated by generating a patch over the axial cross-sections.

origin at the center of the bone. The cross sections were then divided into six equal sectors in the θ direction. With five layers in the radial direction, each cross-section thus contained 30 patches. Bi-cubic hyperpatches were generated by combining corresponding patches from four neighboring cross-sections. The hyperpatches, which are the 3-D equivalent of the patches, followed the same pattern as the patches in maintaining the layered structure of the model. Four neighboring cross-sections containing 30 patches each were combined into a slice of finite width containing 30 hyperpatches. Continuity in surface slopes was imposed on any two adjacent hyperpatches to ensure a smooth geometry suitable for the generation of higher order finite elements. It should be noted that the geometry definition was completely distinct from the finite-element mesh so as to test different meshing schemes. The specification of the material properties could also be selected independent of the geometry and the mesh definition.

Finite-element meshes were then generated by defining nodal points within the hyperpatches, using Patran software. Figure 4 shows a perspective view of the monkey and human fingertip models with the hidden lines removed. The model shown contains eight-node isoparametric elements for the fingertip and four-node membrane elements for the fingernail. The finite-element analyses were performed using Abaqus software (Pawtucket, RI). The boundary conditions were specified by rigidly fixing all the nodes corresponding to the nail portion of the finger, since the fingernail was always glued to the table in the biomechanical and neurophysiological experiments that the analysis simulated. Because of the irregular geometry of the fingertip and features that vary in size by orders of magnitude, together with the conflicting requirements of higher resolution and lower computational effort, an optimal meshing scheme was required. High spatial resolution was sought in the vicinity of the mechanoreceptors (generally the top 2 mm), so that spatial resolution finer than the receptor spacing in the actual fingertip could be obtained. The stimuli in all the biomechanical and neurophysiological experiments relevant to the analysis described here were delivered on the fingerpad. Hence, finer mesh size is required on the fingerpad skin (on the glabrous side) to accurately simulate the mechanistic interaction of the fingertip with various indentors used in the experiments. Also, it is desirable to have elements with aspect ratio close to unity in the region where loads are prescribed and the region where the stress-state is computed. Custom programs were written in the Patran Command Language to test various meshing schemes that allowed the mesh to be varied in the radial and axial direction, while satisfying other requirements. The final choice was made considering the fact that the model would be used in the solution of several iterative nonlinear contact problems in the simulation of some neurophysiological experiments involving complex object

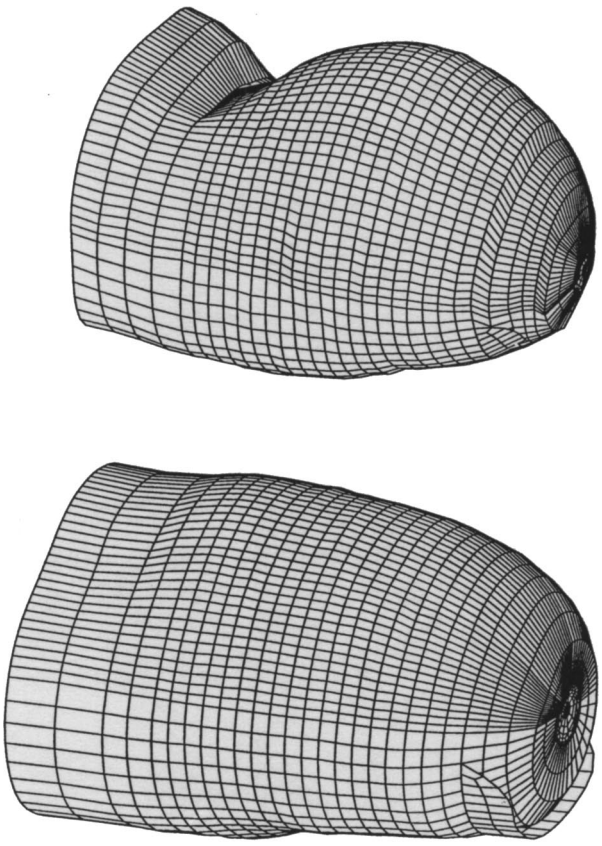

Fig. 4 3-D view of the monkey (top) and human (bottom) fingertip meshes along with the nail. The hidden lines are removed for clarity. The scale is not the same for the two fingertips (monkey fingertip width ~8–10 mm; human fingertip width ~16–20 mm).

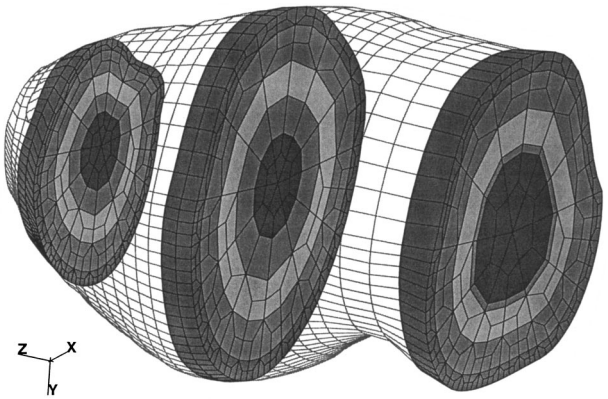

Fig. 5 Three slices of the monkey fingertip model are shown. The elements are shaded to show the five layers used in the model.

shapes. For the monkey fingertip, two finite-element models were developed. The first one had about 8500 nodes and the second one had about 29,000 nodes. Both these models were the same except for the difference in mesh density. For the human fingertip, only one finite-element model with about 8500 nodes was developed.

Figure 5 shows three different cross sections of the 8500-node monkey fingertip model in relation to the entire fingertip. The nail is not shown here for clarity. In the cross-sections, the different layers are indicated by different shades of gray. It can be seen that smaller elements were used on the fingerpad surface (the bottom part in Fig. 5). The typical width of monkey fingertips was about 8 mm and the element size in the region of contact with indentors was approximately 0.5 mm for this model. It can also be seen that the size of the elements increased in the proximal direction along the axis of the fingertip and, thus, the rightmost slice has only one element in the axial direction, whereas the other two slices have two elements each for the same thickness. The transition scheme used increases the size of the elements by a factor of 2 in the radially inward direction with every layer of the transition elements. The geometry of the transition elements is suitable to model the epidermal and dermo-epidermal ridges with the proper assignment of material properties to distinguish between the layers of the skin. This model was used in determining the material properties of the layers by matching model predictions with empirical data from Srinivasan [3]. This model was also used to show the capability of an inhomogeneous material model of the fingertip to predict the neural response of SA-I mechanoreceptors to indentation by sinusoidally shaped indentors [11].

The higher-resolution model (29,000 nodes) was developed in order to simulate the experiments of Phillips and Johnson [4] wherein gratings with edges were indented onto the monkey fingerpad at successive locations. Higher-mesh resolution was required because in order to simulate contact by sharp edges, the element size must be much smaller than the distance between two successive edges. For this high-resolution model the element size in the contact region was 0.17 mm, about one third of that for the lower-resolution model. Since simulating the full neurophysiological experiment would be computationally expensive, especially with this high-resolution model, it was decided to simulate only a portion of the experiment, namely indentation by an isolated 3 mm wide bar.

4 Determination of Material Properties

Although the external geometry of both the macaque monkey and human fingertip models developed here is accurate and the internal geometry approximates the major tissue layers, no consistent in vivo data are available on the material properties of the different tissue layers. Our approach was to start with the simplest material model, namely, that of linear isotropic elasticity, for which two constants (elastic modulus and Poisson's ratio) need to be specified. Since soft tissues are generally considered incompressible owing to their predominant fluid content, the Poisson's ratio was assumed to be 0.48, close to the theoretical limit of 0.5 [12–14]. Consistent with the systems modeling approach followed here, to obtain optimal values of the elastic moduli for the different layers, numerical exploration was done to obtain a match between the model predictions and available empirical data. At first, the ratio of the elastic moduli of the various layers were determined by matching skin surface deflection profiles under line loads indenting the human and monkey fingertips to various depths of indentation obtained by Srinivasan [3]. As in the experiments conducted previously, the fingertip models were indented by a sharp wedge aligned perpendicular to the finger axis up to a depth of 2.0 mm in steps of 0.5 mm, with displacements prescribed on the nodes under the wedge to simulate the indentation. Since the loading, boundary conditions, and the desired surface deflection profiles are all in terms of displacements, numerical values of the elastic moduli of the soft tissues and bone were not necessary in this analysis [2]. Only the ratio of the moduli for the various layers was sufficient to uniquely compute the displacements and the strains in the models.

4.1 Homogeneous Models

To begin with, all the soft tissue layers of the model were assigned identical elastic moduli and the modulus for the bone was chosen to be five orders of magnitude higher. Thus, this model is the 3-D counterpart of the earlier cylindrical model composed of homogeneous soft tissues and a rigid bone [2], and will be referred to as the homogeneous model The extent of the deformation can be seen from the deformed mesh in Fig. 6, where contours of constant vertical displacement are shown overlaid on the monkey and human fingertip models. It can be seen that even at a depth of indentation of 2.0 mm, the deformations rapidly decrease with distance from the line load. There is considerable difference in the dimensions of the monkey and human fingertips: the macaque monkey fingertips are 8–10 mm in diameter whereas the human fingertips are typically 16–20 mm in diameter. There is also a difference in the curvature of the fingertips: it can be seen that the monkey fingertips are more ellipsoidal whereas the human fingertips are more cylindrical. In spite of the differences in the sizes of the fingertips, the overall shape and the internal structure of the primate fingertips are similar, and consequently the predicted vertical displacements are also similar in the two models.

Figure 7 compares the deformations predicted by the homogeneous 3-D models with the corresponding experimental data. It shows that in spite of calculating the displacements using the 3-D model that is geometrically accurate, the predicted displacements do not match the experimentally observed displacements. Hence, as was the case with the 2-D homogeneous model [2], the 3-D homogeneous model is inadequate in predicting the biomechanical behavior of the primate fingertip. We next examined the hypothesis that it is essential to take into account the multiple tissue layers that make up the fingertip.

4.2 Multi-Layered Models

Using the five layers of the finite-element model, a parametric study was undertaken to study the effect of changing the elastic modulus of a particular layer on the overall surface deformation profile. The elastic modulus of the layer corresponding to the bone was held constant at least three orders of magnitude higher than that of any other layer of the fingertip. For convenience, the different layers in the model were numbered radially inward, with layer 1 corresponding to the skin and layer five corresponding to the bone. Layers one through four were assigned elastic moduli in powers of 10 and, hence, it was possible to represent a model by collating the logarithms of the elastic moduli of all the layers. For example, a model designated by m43328 had the elastic moduli ratios of $10^4:10^3:10^3:10^2:10^8$ for the layers of the model starting

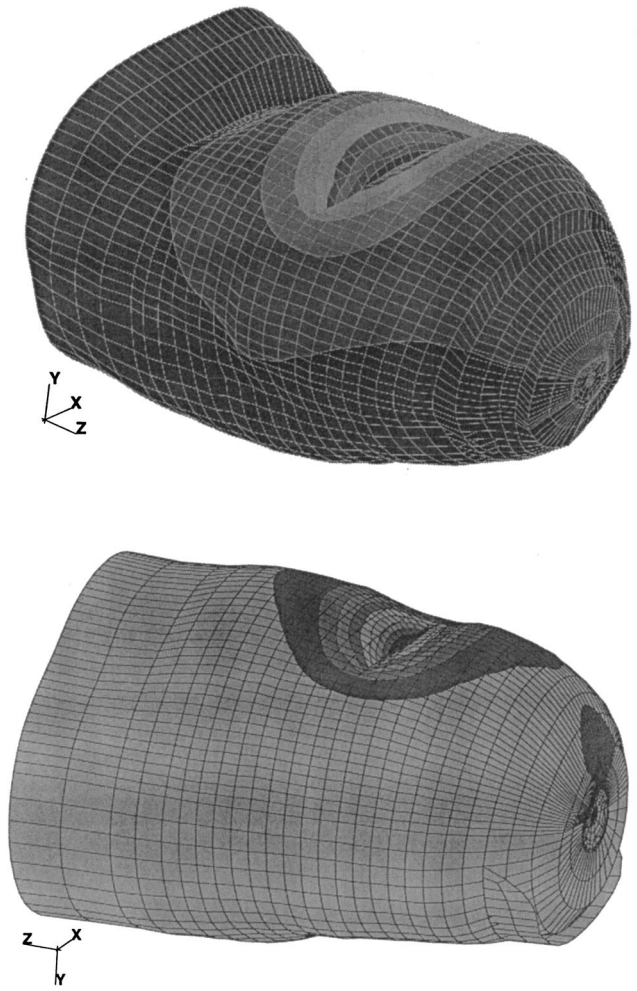

Fig. 6 Deformed meshes of the monkey (top) and human (bottom) fingertips indented by a sharp wedge aligned perpendicular to the axis of the finger. The wedge was indented into the fingertip up to a depth of 2.0 mm in increments of 0.5 mm. The contours of constant vertical displacement (in steps of 0.2 mm) of the fingertips under 2 mm indentation by the line load are shown.

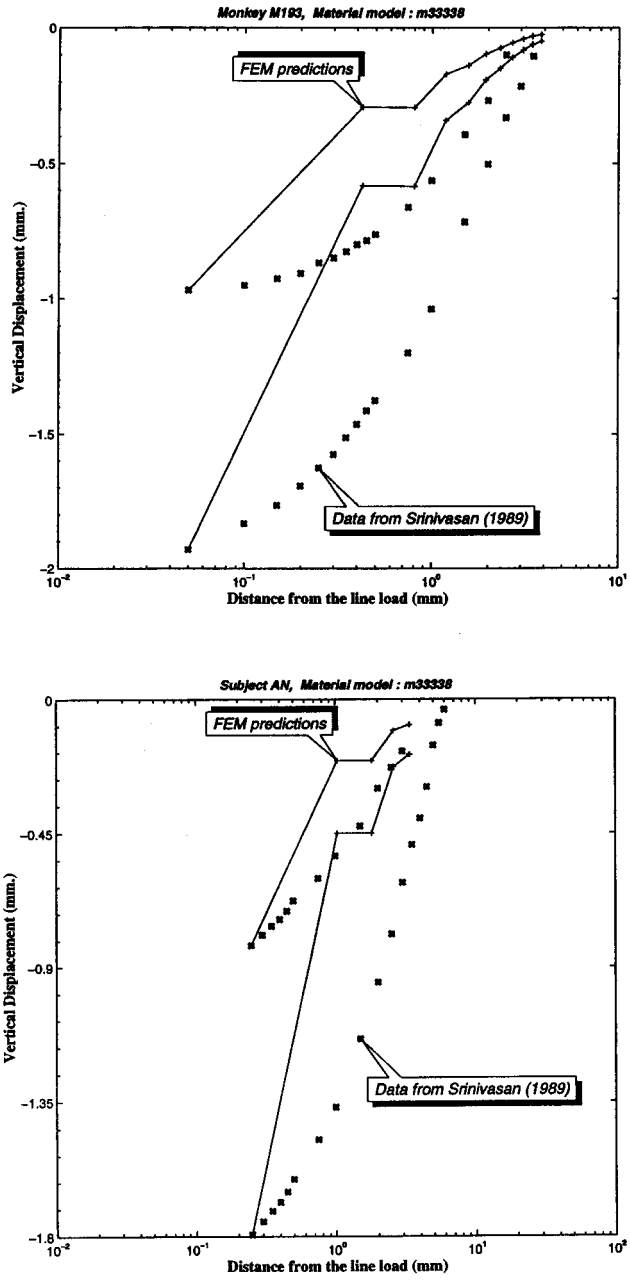

Fig. 7 Surface deformation predicted by the homogeneous monkey (top) and human (bottom) fingertip models are compared with the experimental data from Srinivasan [3]. The element size for the monkey and human models were approximately 0.4 and 0.8 mm, respectively. Vertical displacements plotted for two depths of indentations of 1 mm and 2 mm show that homogeneous models do not accurately model the biomechanical behavior of the fingertips.

from the outer layer of skin and proceeding to the bone. The results of this study are summarized in Fig. 8. In all the sub-plots, experimental data obtained by Srinivasan [3] for a monkey fingertip were used for comparison with the model predictions.

The top panel in Fig. 8 shows the effect of changing the stiffness of the outermost layer, which corresponds to that of the epidermis. As the stiffness of this layer is increased, the spatial extent of the deformation increases. The trace corresponding to the model m33338 is identical to the result for the homogeneous model described earlier in Fig. 7 and shows mostly local deformation near the line load. If the stiffness of the outermost layer is decreased (model m23338, symbol: +), the spatial extent of the deformation further reduces and the deformation is even more localized and thereby increases the error between the experimental and the predicted data. On the other hand, if the topmost layer is stiffened by increasing its elastic modulus (models m43338 and m53338), only the surface deformation predicted by the m43338 model matches the experimentally determined deformation.

In the second panel, the effect of layer two shows a mixed trend: as its stiffness increases, the deformation is more localized for distances less than 1.25 mm from the load, but the opposite is true for larger distances. Nevertheless, the overall effect of this layer's stiffness on deformation is much less than that of the first layer. In the case of layer three as well as layer four, an increase in stiffness causes a decrease in the extent of the deformation, or, equivalently, the deformation is more local. At a given distance from the load, if the spread among various traces is viewed as the effect of the corresponding layer's stiffness, a general observation is that the deeper the layer, the region most affected is farther from the load. Also, the deformation is most affected by layer one and least by layer two. These findings essentially provide us with a systematic procedure for adjusting the model parameters to match the observed displacement data. From all the panels in Fig. 8, m43338 and m43238 show the most promise in accurately pre-

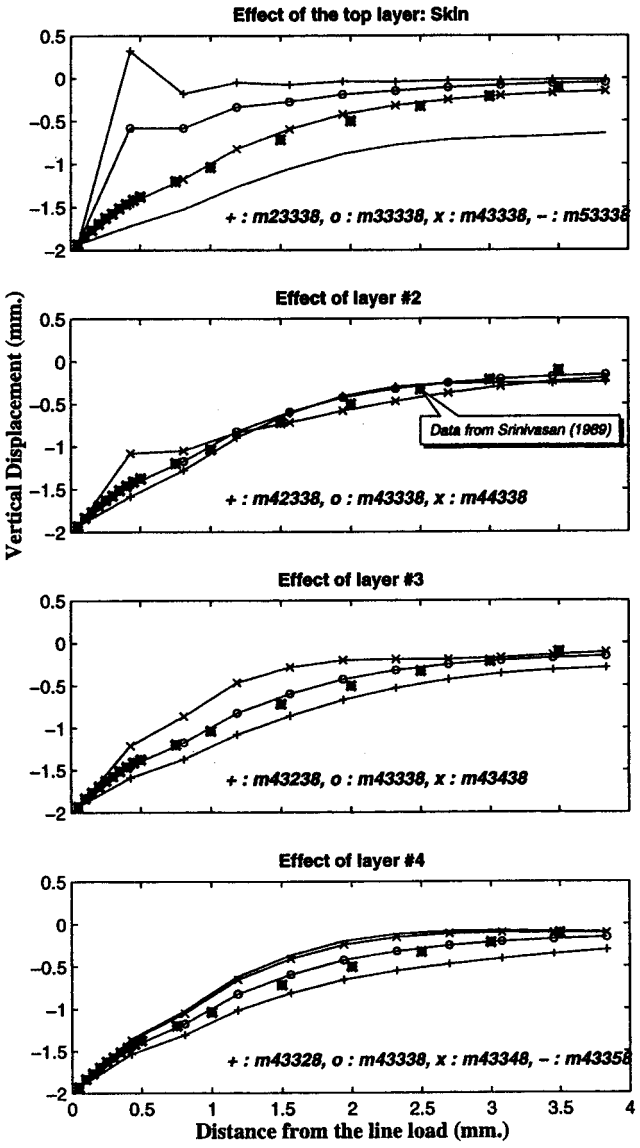

Fig. 8 Effect of layer stiffness on the surface deformation. The elastic modulus of the bone was held constant at 10^8 and the elastic moduli of other layers were varied successively by a factor of 10. The predicted vertical displacement is compared with the experimentally observed data for a monkey fingertip indented to a depth of 2.0 mm.

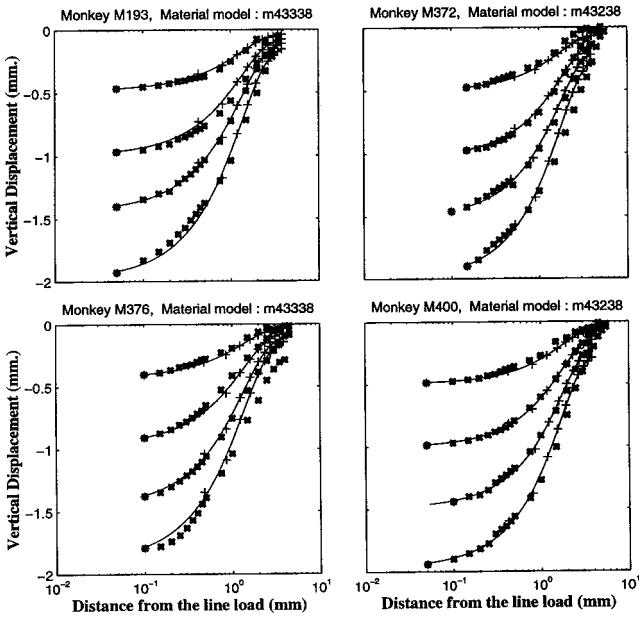

Fig. 9 Surface deformation of the monkey fingertip under line loads predicted by the finite-element model and comparison with observed surface profile data for four monkey fingertips, each indented to 4 different depths (0.5 mm to 2.0 mm at 0.5 mm steps). The empirical data from Srinivasan [3] are shown with crosses and the finite-element predictions are shown by solid lines. For each monkey fingertip, the material model used in the finite-element models is listed on the top of the plot.

dicting the observed surface deformations. Therefore, the homogeneous model was modified by increasing the elastic modulus of the outermost layer to 10^4, and the effect of layer three was analyzed in more detail.

For each monkey and human subject, several combinations of the ratios of elastic moduli of different layers were analyzed and the predicted surface deformations were compared with the empirically determined deformation profiles at different depths of line load indentations. Matches and mismatches between the two sets of profiles, along with the guidelines for changing the material parameters depending on the region of the mismatch as discussed earlier, were used to successively modify the materials of the various layers. Figure 9 shows the comparison of the predicted surface deformation with the experimentally observed data for the best material model for each of the monkey fingers. The excellent match between the observed and predicted data is clearly seen. In all the cases, the stiffness of the outermost layer was higher than those of the inner layers. In the cases of monkeys M372 and M400 (right panels in Fig. 9), the best match was obtained with the middle layer being more compliant than layers two and four. These results show that a three-layer model consisting of a stiff outer layer, a compliant middle region, and a rigid bone is adequate to accurately predict the surface deformations under a line load. Because of the variability in both geometric and material properties, individual differences are to be expected between subjects and between different fingertips of the same subject. There is evidence to suggest that the epidermis is stiffer than the dermis in its mechanistic behavior [15]. In the three-layered model, the effects of the skin are lumped in the stiff outer layer, the adipose tissue and the ground substance are modeled as the middle layer, and the bone is modeled as the innermost layer, which is several orders of magnitude stiffer than the rest of the fingertip and, hence, can be treated as rigid.

A three-layered model m43338 was developed for human fingertip geometry as well and was used to predict the deformations under a line load for the human fingertips. The comparison of the experimentally observed and predicted deformations is shown in Fig. 10. The finite-element model predicts the surface deformations under the line load very well. As in the case of monkey fingertips, a three-layer model is adequate to predict the surface deformations of the human fingertips under a line load. Interestingly, as in the case of monkey fingertips, even though the human data is from three different subjects, a single finite-element model was used to predict the surface deformations. There is no free parameter in the model and no curve fitting was performed before plotting the data in Figs. 9 and 10. The excellent agreement between the observed and predicted data confirms that taking into account the inhomogeneity in the primate fingertip through an appropriate multi-layer model is of primary importance in predicting the surface deformation under a line load for monkey and human fingertips and the geometrical differences between the individual subjects have a secondary effect on the observed surface deformations.

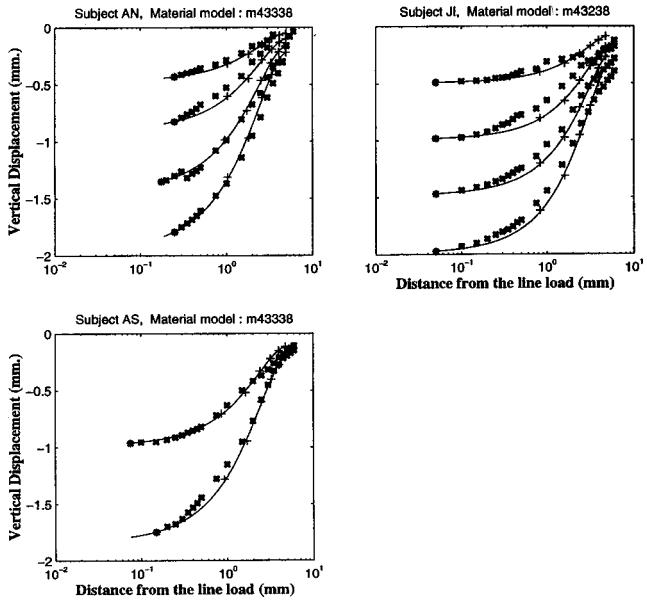

Fig. 10 Surface deformation of the human fingertip under line loads predicted by the finite-element model. The empirical data shown with crosses for three human subjects is from Srinivasan [3]. Same format as Fig. 9.

4.3 Determination of the Numerical Values of the Elastic Moduli

In order to determine the numerical values of the elastic moduli of the various layers, empirically determined force-displacement response of the fingertip to various types of indentors were used. The numerical values of the elastic moduli in the model were adjusted while maintaining the 10:1 ratio between the outer and middle layers, such that the predicted force-displacement measures matched the empirically observed data. The elastic modulus of the bone was fixed at four orders of magnitude higher than that of the outer layer. Four sets of data were used for this purpose, two each for human and monkey fingertips. For the human fingertip model, force-displacement data for the case of point and flat-plate indentors obtained by Gulati and Srinivasan [16] were used. In these experiments, index fingers of five human subjects were indented up to several prescribed displacements, and the force-displacement data corresponding to 1 mm indentation were used to determine the numerical values of the elastic moduli. For the monkey fingertip model, data from Srinivasan and LaMotte [11] and additional line load data previously unreported were used. In the experiments by Srinivasan and LaMotte [11], various step shaped indentors were indented up to a prescribed force and the resulting displacements were measured. Data corresponding to the indentations up to about 7–8 grams by the flat-plate portions of these step shapes were used in the present study. The additional experiments on the monkey using line load indentors were obtained using a system that was designed for a separate study. Briefly, the setup consisted of a three-axis motion platform on which a motor with a displacement transducer and a system for force control (Model 305B, Aurora Scientific, Ontario, Canada) was mounted. An indentor fixed to the motor applied a line load to the finger, with the load applied along the finger axis. Three prescribed force of indentation experiments were done on macaque monkeys and the corresponding displacements were measured. Tables 1 and 2 summarize the experiments and results for both the human and monkey models. On the average, the epidermal elastic moduli that best matched the human and monkey data were 0.18 and 0.14 MPa, respectively. With the determination of the numerical values of the elastic constants of the three layers, the model specification is complete.

Table 1 Elastic modulus of in vivo human epidermis in the finite-element model. Both the point and flat-plate indentation data were taken from Gulati and Srinivasan [16].

Indentor	Subject #	Force (grams)	Displacement (mm)	Elastic modulus of epidermis (MPa)
Point load indented up to 1 mm	1	5.29	1.0	0.28
	2	2.74	1.0	0.14
	3	3.34	1.0	0.17
	4	2.65	1.0	0.14
	5	4.55	1.0	0.24
Flat plate indented up to 1 mm	1	23.59	1.0	0.21
	2	24.73	1.0	0.23
	3	11.82	1.0	0.11
	4	17.46	1.0	0.16
	5	13.35	1.0	0.12
			Mean±SD	0.18±0.06

5 Prediction of Skin Mechanoreceptor Response

The main goal for the development of the 3-D human and monkey finite-element models in this paper is to gain a deeper understanding of the mechanistic bases of the human sense of touch. In particular, it needs to be verified if the model developed is capable of predicting the known mechanoreceptor response to object shapes in contact with the skin. We now show some examples of the relevance of the models to predicting tactile neural response.

Table 2 Elastic modulus of monkey epidermis in the finite-element model. The flat-plate data were obtained from the experiments done by Srinivasan and LaMotte [11].

Indentor	Monkey #	Force (grams)	Displacement (mm)	Elastic modulus of epidermis (MPa)
Line load indented up to the prescribed force	MK1, alive, right index finger	5.0	0.66	0.22
	MK1, alive, left index finger	5.0	1.14	0.10
	MK2, 3 hours post mortem, right index finger	3.4	1.05	0.08
Flat plate indented up to a prescribed force, approximately 8 grams	A, alive	7.48	0.78	0.15
	B, alive	7.66	0.80	0.15
	C, alive	7.30	0.79	0.14
	D, alive	6.91	0.80	0.14
			Mean±SD	0.14±0.05

5.1 Rectangular Bar Indentor

Phillips and Johnson [4] obtained neurophysiological data on the responses of SA-I afferents to several gratings indenting the monkey fingerpad. In these experiments, the responses of single SA-I fibers were recorded for a sequence of indentations by moving the indentor laterally between the indentations. The responses were then plotted as a function of the spatial location on the grating to obtain the spatial response profile of the SA-I fiber. A portion of the above experiment was simulated using the high-resolution finite-element FE model. To limit the computational effort to a manageable level, indentions by an isolated portion of the grating, namely a rectangular bar of 3 mm width were studied. The high-resolution model was used in order to better simulate indentations by the sharp edges in the bar. Totally 35 indentations were done for successive locations of the indentor, and various mechanical quantities including all the tensorial stress and strain components were obtained for each indentation. Results were obtained for the layered model with elastic properties described in the previous section, as well as the homogeneous model with a single material for all the layers except bone. The stress and strain measures were fitted to the experimentally recorded neural responses using a simple scaling and threshold model as done by Phillips and Johnson [4]. Figure 11 shows the results for four quantities, strain energy density, maximum compressive strain, mean normal stress, and vertical compressive stress. The correlation coefficients for the layered model were higher than that for the homogeneous model for all the quantities. In the case of strain energy density and maximum compressive strain, the layered model prediction shows the dip in the recorded data better. Also the locations of the two peaks match that of the experimental data better for the layered model than for the homogeneous model. Among the four quantities shown, both mean normal stress and vertical compressive stress were unable to model the recorded neural data well, and strain energy density showed the highest correlation coefficient. Even in our previous study with a 2-D model, strain energy density was shown to be the likely strain measure coded by the mechanoreceptors [2]. It should also be pointed out that because the edges of the bar are perfect corners, the finiteness in mesh resolution is a limitation even with the high-resolution model, and therefore the dips seen in the predicted neural responses are not as much as the experimentally recorded data. As the element size reduces even further, we expect that the match between the model predictions and recorded data would improve.

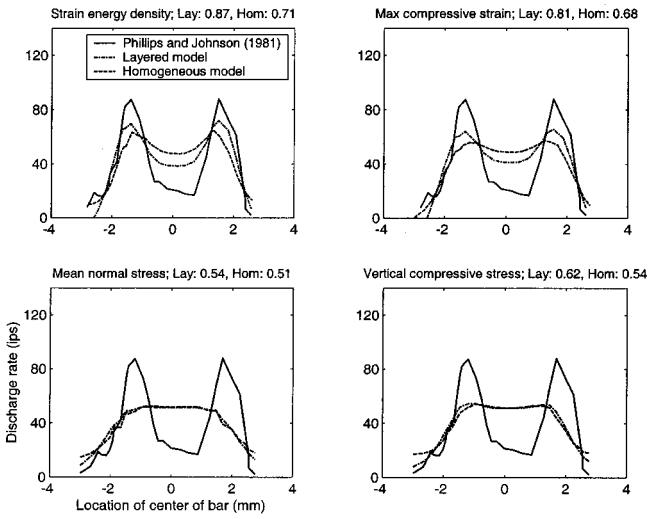

Fig. 11 Neural response of an SA-I afferent to indentation by a 3 mm-wide rectangular bar predicted by the high-resolution monkey fingertip model based on four candidate mechanical quantities: strain energy density, maximum compressive strain, mean normal stress, and vertical compressive stress. The quantities were computed for both the layered and the homogeneous models. The *x* axis is the location of the center of the bar as it was indented at various locations on the fingerpad. The numbers above each panel indicate the correlation coefficient between the recorded neural response and the predicted response for each mechanical quantity for the layered ("lay") and homogeneous ("hom") models. The layered model was able to model the neural response better than the homogeneous model for all the four quantities. Strain energy density was able to predict the neural response better than the other quantities.

5.2 Sinusoidal Step Shapes

Srinivasan and LaMotte [11] obtained neurophysiological data on the responses of slowly adapting type I (SA-I) afferents to several sinusoidally shaped objects (referred to as step shapes) indenting the monkey fingerpad. In these experiments, the responses of single SAI fibers were recorded to sequential indentations by a step shape such that the monkey fingerpad came in contact with successive spatial locations on the step shape. The responses were then plotted as a function of the spatial location on the step to obtain the spatial response profile of the SA-I to each step. The same procedure was simulated on the monkey fingertip model for three of the step shapes (steps 1, 3 and 5) by taking into account the contact mechanics in the finite element analysis. The step shapes consisted of two flat surfaces separated by a half sinusoid whose wavelength varied among the three steps. The 8500-node model was used as the indentors did not have sharp edges as in the case of the rectangular bar. As in the neurophysiological experiments, between two indentations the step was laterally shifted by 0.1 or 0.2 mm depending on the curvature of the step. For all the indentations among the three steps, it was found that the higher the contact area, the lower the maximum contact pressure within the contact area, and vice versa. Figure 12 shows the results for the case of step 5. When the convex portion of the indentor was in contact with the finger, the contact area was mini-

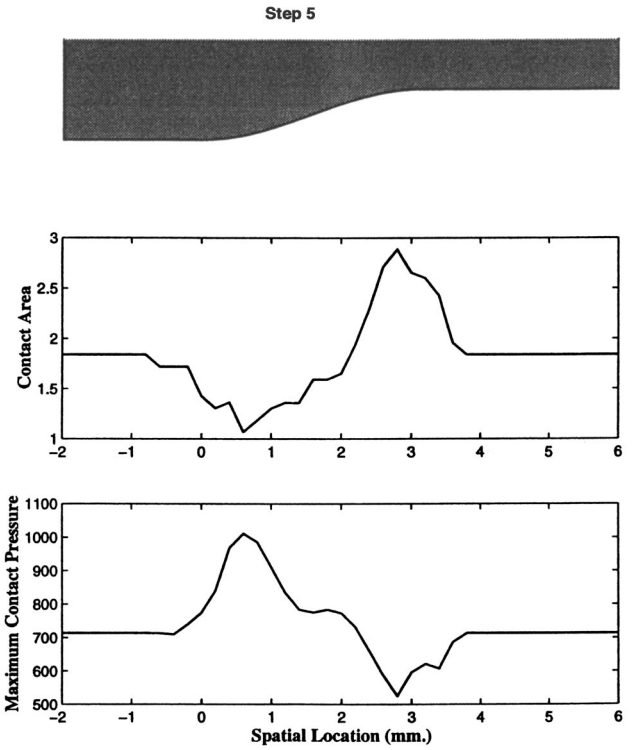

Fig. 12 The variation in contact area and maximum contact pressure for constant force of indentation of step 5 at various locations on the monkey fingertip model

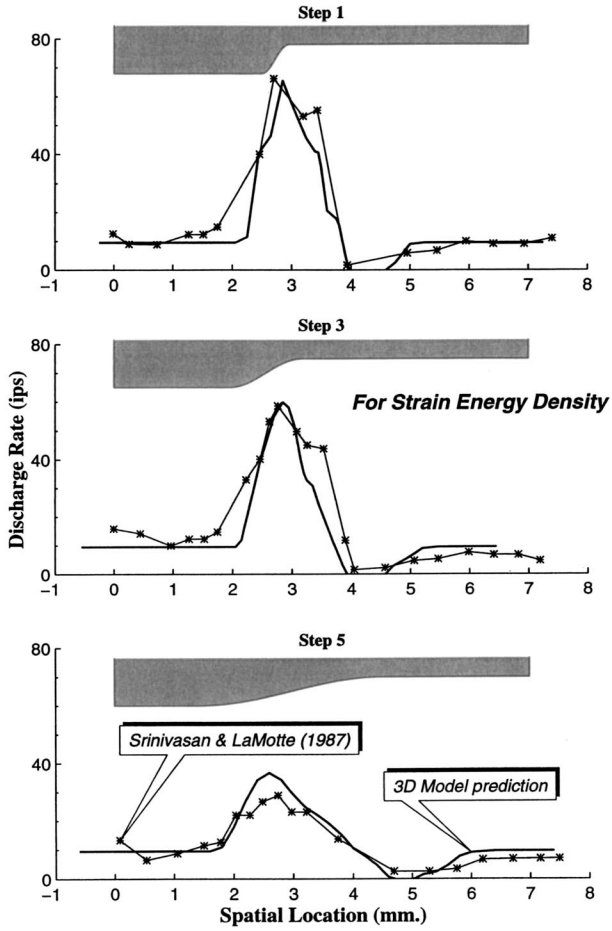

Fig. 13 Neural response of SA-I afferent to indentation by step shapes predicted by the monkey fingertip model. Strain energy density computed at a typical receptor location (0.75 mm below the skin surface) is matched with spatial response profiles recorded previously by Srinivasan and LaMotte [11]. Good fits between the predicted and measured data (same scaling and threshold values for all the three step shapes) indicate that strain energy density is a good candidate be the relevant stimulus for SA-I mechanoreceptors.

mum, and the contact pressure was maximum. When the concave part of the step was over the fingertip, the contact area was the highest and was accompanied by the lowest magnitude of the maximum pressure within the contact region.

Neurophysiological data from one SA-I afferent [11] was matched with strain energy density computed at the receptor location using a single set of scaling and threshold parameters. For the assumed linear relationship between suprathreshold values of strain energy density at the receptor location and the neural discharge rate to be valid, a single set of scaling and threshold parameters should be able to predict the neural response from a single mechanoreceptive afferent fiber under all the three step shapes. Figure 13 shows the comparison between the experimentally observed and the predicted data. The spatial response profile of the SA-I is generated by plotting the evoked discharge rate as a function of the step position and the corresponding strain energy density calculated at a typical receptor location (0.75 mm below the skin surface) is also plotted as a function of the step position. The same scaling and threshold parameters obtained for the best fit between the experimental data for step 1 and the corresponding strain energy density were then used to predict the response when the fingertip was indented by steps 3 and 5. By comparing neural data from one afferent unit, with the stress-state at a unique receptor location using the same set of fitting parameters, we are verifying the combination of the biomechanical and neurophysiological models. It is seen that for all the three step shapes that contain concave, flat and convex portions and span steep to gradual shape changes, the model predictions match the experimental data quite well.

6 Discussion

Quantitative understanding of the mechanisms underlying the human sense of touch is important from both basic scientific point of view as well as for applications such as robotics, rehabilitation, virtual reality, and development of tactile displays. Given the experimental limitations in directly observing the associated tissue deformations and stresses at sufficient resolution, mechanistic models of the skin and tissues underneath are needed. Since the structure and material behavior of the primate fingertip are quite complex at many spatial and temporal scales, the models necessarily have to be approximate to a considerable degree. We have therefore followed a systems approach where the input—output behavior of the model is validated by matching it with the corresponding experimental data. Only when the experimental data demands more complexity, finer features of the fingertip should be incorporated into the model. This approach ensures minimal number of model parameters to predict or match available experimental data.

Our earlier papers on 2-D models have shown that both the geometry of the fingertip and its multi-layered structure are important in modeling the mechanical behavior of the primate fingertip [2]. The results obtained with 3-D models in this paper confirm this as well: even when the external geometry was accurate, the homogeneous model failed to predict the deformation data under line load, and necessitated a multilayered model. A model with skin being an order of magnitude stiffer than the soft tissues underneath and the bone being relatively rigid has been shown to be sufficiently accurate. The multi-layered model was also able to predict the recorded neural data better than the homogeneous model. We have assumed that the skin and fingertip tissues can be described by a linear stress-strain mechanical behavior. As shown by earlier studies, the elastic behavior of skin is nonlinear and can be divided into three regions: an initial region of low elastic modulus, a transition region, and a final region with high elasticity [15,17,18].

The small value of the small-deformation elastic modulus (initial slope) of the skin is required to permit normal joint movements, whereas the larger value of the large-deformation elastic modulus is needed to provide mechanical strength [19]. Because of the relatively small forces used during typical tactile explorations, the low elasticity values are more relevant for our purposes, and consequently we have used only small depths of indentations in our simulations to determine the material properties. The assumption of linear elasticity was also based on the need to keep the model simple and tractable without too many curve-fitting parameters. A direct comparison of our numerical values with values from the literature for the small-deformations elastic modulus of the skin is not possible due to various reasons: differences between in vitro and in vivo conditions, various assumptions made in previous in vivo measurements (e.g., effect of underlying tissue, and the measurement of skin thickness in the extensometer and suction methods), and differences in the animals and body sites chosen for testing. Moreover, in our work we have considered the epidermis and dermis to be separate tissues, because the mechanoreceptors are mainly located in the dermis. Table 3 shows a summary of the elastic modulus of skin tissues available in the literature. Our results are close to that obtained by Maeno et al. [8] for fingertip skin. It should also be pointed out that the nonlinear force-displacement response observed during fingertip indentation studies [7,16,20] has contributions from large deformation nonlinear strain-displacement relationships as well as contact nonlinearities, and are not necessarily indicative of nonlinear material behavior.

Table 3 Comparison of literature values for the small-deformation elastic modulus of skin tissues

Reference	Tissue	Method	Small-deformation elastic modulus (MPa)	Notes
Grahame [22]	Human, in vivo, back of forearm	Suction method	2.5	Estimated from Fig. 3
Veronda and Westmann [23]	Cat, in vitro	Unaxial testing	0.5	Estimated from Fig. 1
Daly [19]	Human abdomen, in vitro	Uniaxial testing	0.005	Mentioned in Fig. 2
Manschot and Brakkee [24]	Human calf, in vivo	Extensometer	0.68 along and 0.17 across tibial axis	Estimated from Fig. 5
Oxlund et al. [25]	Rat, in vitro	Uniaxial testing	0.24	Mentioned in Table 1
Pan et al. [26]	Human forearm, in vivo	Extensometer	0.035	Mentioned in text
Maeno et al. [8]	Human cadaver finger	Matching 2D FE results with load-displacement data	0.136 (epidermis) 0.08 (dermis)	Mentioned in Fig. 7
This study	Human and monkey fingertip in vivo	Matching 3D FE results with load-displacement data	Epidermis: 0.18 (human) 0.14 (monkey) Dermis: 0.018 (human) 0.014 (monkey)	

In this paper, in addition to matching biomechanical data, the monkey fingertip model was also shown to predict the SA-I neural response to relatively complex shapes. It has been observed previously that the SA-I responses are highly sensitive to the curvature of the object [4,11]. The current simulations support the mechanism for neural encoding of shape suggested by Srinivasan and LaMotte [21]. As the curvature of the object increases gradually from concave values to zero curvature (flat plate) and further to convex values, when the force of indentation is kept constant, the contact region decreases and the peak pressure increases. For SA-I fibers, since the associated mechanoreceptors are very close to the surface, an increase in pressure directly results in increased deformation as well as stresses and strains at the receptor locations and consequently in increased receptor response. The skin effectively acts as a spatial low-pass filter in transmitting the mechanical signals, and the mechanoreceptors respond to the blurred versions of the surface pressure distribution, thus encoding the shape of the object in terms of its surface curvatures.

The models developed here have been validated for static biomechanical and neural data. Further studies in this area could include the incorporation of viscoelastic properties for simulation of dynamic loads, the determination of relevant stimuli for various types of mechanoreceptors in skin, and the determination of the effects of finger ridges in tactile neural coding.

Acknowledgments

This research was supported by grants from National Institute of Neurological Disorders and Stroke (NS33778) and the NSF Pittsburgh Supercomputer Center. The authors would like to thank Prof. Robert LaMotte and Dr. S. James Biggs for making available the monkey line load force-displacement data.

References

[1] Lanir, Y., 1987, ''Skin Mechanics,'' In: *Handbook of Bioengineering*, McGraw-Hill, New York.
[2] Srinivasan, M. A., and Dandekar, K., 1996, ''An Investigation of the Mechanics of Tactile Sense Using Two-Dimensional Models of the Primate Fingertip,'' J. Biomech. Eng., **118**, pp. 48–55.
[3] Srinivasan, M. A., 1989, ''Surface Deflection of Primate Fingertip Under Line Load,'' J. Biomech., **22**, pp. 343–349.
[4] Phillips, J. R., and Johnson, K. O., 1981, ''Tactile Spatial Resolution. II. Neural Representation of Bars, Edges, and Gratings in Monkey Primary Afferents,'' J. Neurophysiol., **46**, pp. 1192–1203.
[5] Phillips, J. R., and Johnson, K. O., 1981, ''Tactile Spatial Resolution. III. A Continuum Mechanics Model of Skin Predicting Mechanoreceptor Responses to Bars, Edges, and Gratings,'' J. Neurophysiol., **46**, pp. 1204–1225.
[6] Serina, E. R., Mockenstrum, E., Mote, C. D., Jr., and Rempel, D., 1998, ''A Structural Model of the Forced Compression of the Fingertip Pulp,'' J. Biomech., **31**, pp. 639–646.
[7] Serina, E. R., Mote, C. D., Jr., and Rempel, D., 1997, ''Force Response of the Fingertip Pulp to Repeated Compression—Effects of Loading Rate, Loading Angle and Anthropometry,'' J. Biomech., **30**, pp. 1035–1040.
[8] Maeno, T., Kobayashi, K., and Yamazaki, N., 1998, ''Relationship Between the Structure of Human Finger Tissue and the Location of Tactile Receptors,'' JSME Int. J., **41**, pp. 94–100.
[9] Maeno, T., and Kobayashi, K., 1998, ''FE Analysis of the Dynamic Characteristics of the Human Finger Pad With Objects With/Without Surface Roughness,'' *Proceedings of the ASME Dynamic Systems and Control Division*, **DSC-64**, pp. 279–286.
[10] Pawluk, D. T. V., and Howe, R. D., 1999, ''Dynamic Lumped Element Response of the Human Fingerpad,'' J. Biomech. Eng., **121**, pp. 178–183.
[11] Srinivasan, M. A., and LaMotte, R. H., 1987, ''Tactile Discrimination of Shape: Responses of Slowly and Rapidly Adapting Mechanoreceptive Afferents to a Step Indented Into the Monkey Fingerpad,'' J. Neurosci., **7**, pp. 1682–1697.
[12] North, J. F., and Gibson, F., 1978, ''Volume Compressibility of Human Abdominal Skin,'' J. Biomech., **11**, pp. 203–207.
[13] Vossoughi, J., and Vaishnav, R. N., 1979, ''Comments on the Paper 'Volume Compressibility of Human Abdominal Skin,''' J. Biomech., **12**, p. 481.
[14] Srinivasan, M. A., Gulati, R. J., and Dandekar, K., 1992, ''In Vivo Compressibility of the Human Fingertip,'' Adv. Bioeng., **22**, pp. 573–576.
[15] Tregear, R. T., 1966, *Physical Functions of Skin*, Academic Press, New York, NY.
[16] Gulati, R. J., and Srinivasan, M. A., 1997, *Determination of Mechanical Properties of the Human Fingerpad in Vivo Using a Tactile Stimulator*, MIT, Research Laboratory of Electronics Technical Report No. 605.
[17] Lanir, Y., and Fung, Y. C., 1974, ''Two-Dimensional Mechanical Properties of Rabbit Skin-II. Experimental Results,'' J. Biomech., **7**, pp. 171–182.
[18] Fung, Y. C., 1993, *Biomechanics: Mechanical Properties of Living Tissues*, Springer-Verlag, New York, NY.
[19] Daly, C. H., 1982, ''Biomechanical Properties of Dermis,'' J. Invest. Dermatol., **79**, pp. 17s–20s.
[20] Pawluk, D. T. V., and Howe, R. D., 1999, ''Dynamic Contact of the Human Fingerpad Against a Flat Surface,'' J. Biomech. Eng., **121**, pp. 605–611.
[21] Srinivasan, M. A., and LaMotte, R. H., 1991, *Encoding of Shape in the Responses of Cutaneous Mechanoreceptors*, In: Information Processing in the Somatosensory System, Eds: O. Franzen and J. Westman, Wenner-Gren International Symposium Series, MacMillan Press.
[22] Grahame, R., 1968, ''Elasticity of Human Skin in Vivo,'' Ann. Phys. Med., **10**, pp. 130–136.
[23] Veronda, D. R., and Westmann, R. A., 1970, ''Mechanical Characterization of Skin-Finite Deformations,'' J. Biomech., **3**, pp. 111–124.
[24] Manschot, J. F. M., and Brakkee, A. J. M., 1986, ''The Measurement and Modelling of the Mechanical Properties of Human Skin In Vivo—I. The Measurement,'' J. Biomech., **19**, pp. 511–515.
[25] Oxlund, H., Manschot, J., and Viidik, A., 1988, ''The Role of Elastin in the Mechanical Properties of Skin,'' J. Biomech., **21**, pp. 213–218.
[26] Pan, L., Zan, L., and Foster, S., 1997, ''In Vivo High-Frequency Ultrasound Assessment of Skin Elasticity,'' Proc.-IEEE Ultrason. Symp., **2**, pp. 1087–1091.